Clinical and radiomic factors for predicting invasiveness in pulmonary ground-glass opacity

YUTAO DANG[1,2], RUOTIAN WANG[1], KUN QIAN[1], JIE LU[3] and YI ZHANG[1]

[1]Department of Thoracic Surgery, Xuanwu Hospital, Capital Medical University, Beijing 100053; [2]Department of Thoracic Surgery, Shijingshan Hospital of Beijing City, Shijingshan Teaching Hospital of Capital Medical University, Beijing 100040; [3]Department of Radiology, Xuanwu Hospital, Capital Medical University, Beijing 100053, P.R. China

Received April 3, 2022; Accepted August 22, 2022

DOI: 10.3892/etm.2022.11621

Abstract. Patients with preinvasive or invasive pulmonary ground-glass opacity (GGO) often face different clinical treatments and prognoses. The present study aimed to identify the invasiveness of pulmonary GGO by analysing clinical and radiomic features. Patients with pulmonary GGOs who were treated between January 2014 and February 2019 were included. Clinical features were collected, while radiomic features were extracted from computed tomography records using the three-dimensional Slicer software. Predictors of GGO invasiveness were selected by least absolute shrinkage and selection operator logistic regression analysis, and receiver operating characteristic (ROC) curves were drawn for each prediction model. A total of 194 patients with pulmonary GGOs were included in the present study. The maximum diameter of the solid component, waveletHLL_ngtdm_Coarseness (P=0.03), waveletLHH_firstorder_Maximum (P<0.01) and waveletLLH_glrlm_LongRunEmphasis (P<0.01) were significant predictors of invasive lung GGOs. The area under the ROC curve (AUC) for the prediction models of clinical features and radiomic features was 0.755 and 0.719, respectively, whereas the AUC for the combined prediction model was 0.864 (95% CI, 0.802-0.926). Finally, a nomogram was established for individualized prediction of invasiveness. The combination of radiomic and clinical features can enable the differentiation between preinvasive and invasive GGOs. The present results can provide some basis for the best choice of treatment in patients with lung GGOs.

Correspondence to: Dr Yi Zhang, Department of Thoracic Surgery, Xuanwu Hospital, Capital Medical University, 45 Changchun Street, Xicheng, Beijing 100053, P.R. China
E-mail: steven9130@sina.com

Key words: pulmonary ground-glass opacity, invasive pulmonary ground-glass opacity, predictive model, nomogram, decision curve analysis

Introduction

The diagnosis rate of pulmonary ground-glass opacity (GGO) has increased significantly with the application of high-resolution chest computed tomography (CT) (1,2). Previous studies have demonstrated that 63-92.6% of persistent GGOs are precancerous lesions or early stage adenocarcinoma (3,4). According to the Internal Association for the Study of Lung Cancer and the American Thoracic Society and European Respiratory Society classification in 2011, adenocarcinoma is classified as atypical adenomatous hyperplasia (AAH), adenocarcinoma *in situ* (AIS), minimally invasive adenocarcinoma (MIA) and invasive adenocarcinoma (IA) (5). Generally, preinvasive GGOs consist of AAH and AIS, whereas MIA and IA are categorized as invasive lesions (6). To date, the treatment of pulmonary GGOs has often been based on CT manifestations and clinical experience. AAH and AIS are pure GGOs (pGGOs) or mixed GGOs featuring a few solid components on chest CT (7,8), and this type of preinvasive nodule often needs close follow-up or limited resection (9,10). Mixed GGOs with more solid components tend to be invasive lesions and often require segmentectomy or lobectomy with lymph node dissection. Following appropriate surgery, compared with the 100% 5-year disease-free survival (DFS) rate associated with AAH and AIS and the ~100% 5-year DFS rate associated with MIA (11), the 5-year DFS rate of patients with IA remains poor, with previous studies reporting values of 70.5-88.0% (12-16). Therefore, the identification of invasiveness of pulmonary GGOs is important for assessing prognosis and for the decision-making process regarding the choice of the optimal clinical treatment.

Radiomics refers to extrapolation of quantitative clinical features from radiology images (17). In oncology, tumour radiomic features measured by analysing imaging data, including nodal shape and volume, as well as intensity and a series of 'texture' features, can be used to investigate the correlation among the diagnosis, prediction and prognosis of patients with cancer (18-20). The purpose of the present study was to determine the invasiveness of GGOs on the basis of the clinical and radiomic features from chest CT.

Patients and methods

Patient selection and grouping. The present study considered for inclusion a total of 268 patients who underwent

surgery for pulmonary GGOs at Xuanwu Hospital (Capital Medical University, Beijing, China) between January 2014 and February 2019 (301 GGOs in total; 2 patients had three GGOs and 29 had two GGOs, while the rest had one GGO). The inclusion criteria were as follows: i) Complete records of the patient clinical characteristics, including sex, age, smoking history, family history of lung cancer and pathological type; ii) complete non-enhanced chest CT data within 2 months of the operation; and iii) final pathology results indicating malignant lesions, including AAH, AIS, MIA and IA. The exclusion criteria were as follows: i) Patients had undergone puncture biopsy, radiotherapy, radiofrequency ablation or other treatment of GGOs before the chest CT examination; and ii) the maximum diameter of GGOs on CT images was >3 cm. After evaluation against the inclusion and exclusion criteria, a total of 184 patients with 194 GGOs were included in the present study.

According to the pathology results, the patients who were ultimately included were divided into two groups: i) The preinvasive GGO group, composed of patients with preinvasive lesions, including AAH and AIS; and ii) the invasive GGO group, composed of patients with invasive lesions, including MIA and IA.

Ethics approval and consent to participate. The present study was approved by the Medical Research Ethics Committee of Shijingshan Hospital of Beijing City (Beijing, China; approval no. 2020-12). All the procedures involving human participants were performed in accordance with the ethical standards of both institutional and national research committees. Written informed consent was obtained before surgery from either the patients or their representatives.

Clinical feature selection. A review of the relevant literature was performed to select clinical predictors of GGO invasiveness. The predictors included age, sex, smoking history, family history [positive family history of lung cancer was defined as having a first-degree relative (parent, sibling or child) with lung cancer], nodule location, pathological type, the maximum diameter of the GGO in the three-dimensional (3D) image [the value of the maximum diameter was consistent with the value of 'original_shape_Maximum3DDiameter', which is a shape-based radiomic feature extracted by 3D Slicer software (version 4.6.2; http://www.slicer.org) and the GGO consolidation (defined as the maximum dimensions of the area of increased opacification that completely obscured the underlying vascular markings). Subsequently, a 2-round Delphi study (21) was performed using online surveys, and age, sex, smoking history, family history and GGO consolidation were ultimately selected as independent predictors.

Chest CT examination and general imaging feature acquisition. All the preoperative chest CT scans were non-enhanced and performed with one of two machines (Sensation Cardiac 64 or Somatom Definition Flash; Siemens Healthineers). All the CT examinations were performed using the following parameters: 120 kVp; pitch, 1.2; 100-200 mAsec; and collimation, 5.0 mm. The chest CT images of the patients were analysed by two radiologists. The largest diameter of the tumour and consolidation components were separately measured on the lung and mediastinal windows. The final result was determined by averaging the results reported by the two radiologists.

CT texture analysis (TA)

Radiomic feature extraction. CT data in DICOM format were imported into 3D-Slicer software. The volume of interest (VOI) was obtained by semiautomatic segmentation using the Segment Editor function. The VOI was then normalized by the NormalizeImageFilter function. Before performing the radiomic feature extraction with SlicerRadiomics (version 2.1.0; https://www.slicer.org/wiki/Documentation/Nightly/Extensions/Radiomics), grey-level discretization and voxel resampling were performed. All the features were calculated with a fixed bin width of 25 HU, and resampling to a voxel size of 0.6x0.6x5.0 mm^3 was applied. The radiomic characteristics were divided into the following 107 original features: i) Shape-based (14 features); ii) grey-level dependence matrix (14 features); iii) first-order statistics (18 features); iv) grey-level co-occurrence matrix (24 features); v) grey-level run-length matrix (16 features); vi) grey-level size zone matrix (16 features); and vii) neighbouring grey tone difference matrix (five features). In addition, eight groups of wavelet features were calculated based on the intensity and texture features of the original image using a wavelet filter. Wavelet features are obtained by transforming domain representations of tumor intensity and textural features. These features were applied as either a high (H) or low pass (L) filter in each of the three dimensions (x-axis, from left to right; y-axis, from posterior to anterior; z-axis, from inferior to superior): Wavelet-LHL, wavelet-LHH, wavelet-HLL, wavelet-LLH, wavelet-HLH, wavelet-HHH, wavelet-HHL and wavelet-LLL (22). Each intensity or texture feature extracted from the volume of interest is subjected to eight ways of wavelet transform, and finally eight sets of wavelet transform features (a total of 744 features) are obtained (23). Therefore, the features are concentrated in different frequency ranges within the tumour volume. The process of radiomic feature extraction was consistent with the methods previously described (24).

Stable radiomic feature selection. To obtain stable radiomic features, each image data point was subjected twice to VOI segmentation and radiomic feature extraction. The intraclass correlation coefficient (ICC) for each radiomic feature was calculated and the stable radiomic features were selected as ICC >0.75.

Selection of prediction factors and establishment of prediction model. The patients enrolled in the present study were divided into training and validation cohorts. Multivariate logistic regression analysis with the backwards method (25) was used to select independent predictors from clinical features, including consolidation, age, family history, sex and smoking history, in the training cohort, and receiver operating characteristic (ROC) curves were plotted. Area under the ROC curve (AUC) values represent the predictive ability of the clinical prediction model. For radiomic features, the minimax concave penalty least absolute shrinkage and selection operator (MCP-LASSO) algorithm and 10-fold cross-validation were used to identify independent predictors for distinguishing

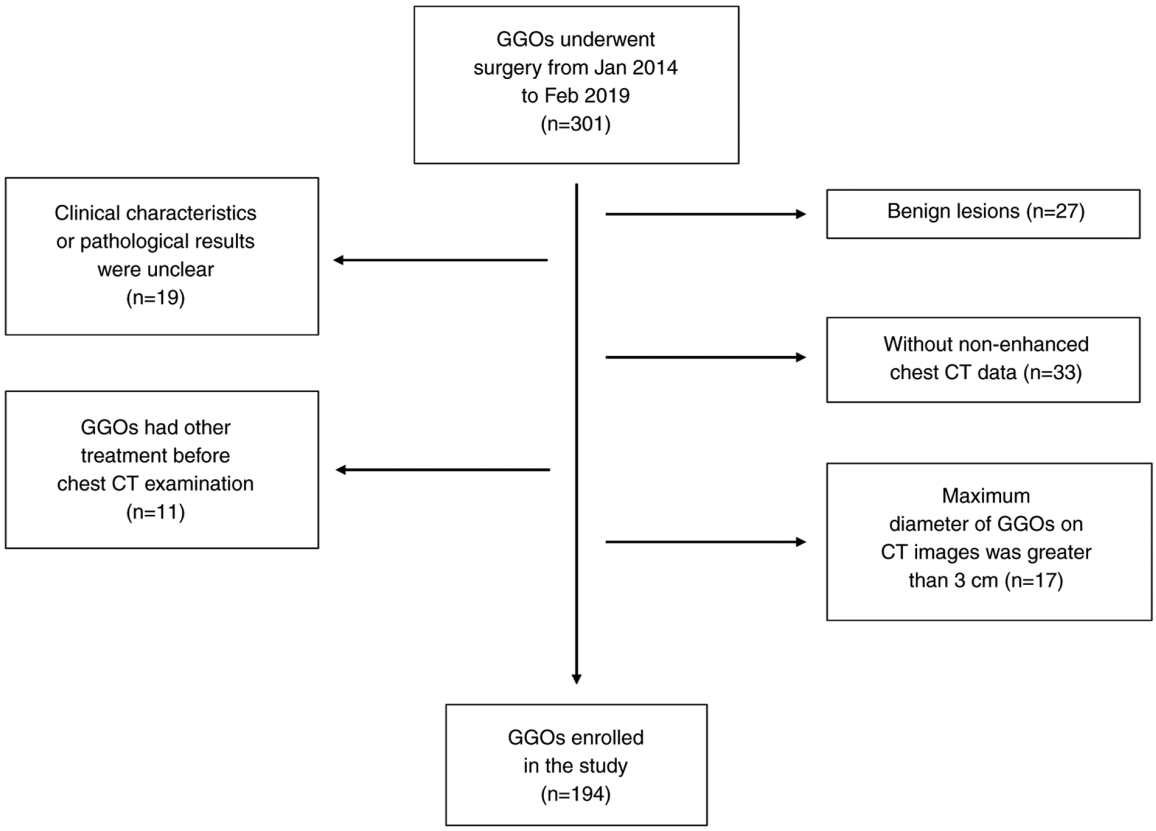

Figure 1. Flow chart of GGO selection. The present study considered a total of 301 GGOs for inclusion. After evaluation against the inclusion and exclusion criteria, a total of 194 GGOs were selected. GGO, ground-glass opacity; CT, computed tomography.

the two pathological subtypes in the training cohort. Next, ROC curves representing the radiomic prediction model were plotted and the AUC values were calculated. Finally, all the meaningful predictors were used to build a combined prediction model, which was compared with the clinical prediction and radiomic prediction models. Moreover, the validation cohort was used to demonstrate the prediction ability of the prediction models. A nomogram was constructed to predict the invasiveness of individual GGOs, and a decision curve analysis (DCA) was performed and plotted.

Statistical analysis. The means of continuous variables were compared using the independent Student's t-test (normally distributed data) or Mann-Whitney U test (non-normally distributed data) and the Pearson χ^2 test was used to analyse differences between categorical variables in two groups using SPSS (version 22.0; IBM Corp.). R software (version 3.5.2; http://www.R-project.org) was also used for data analysis. ICC was calculated using the 'psych' package (version 1.9.12.31; https://personality-project.org/r/psych) in R. The 'MASS' package (version 7.3-51.4; http://cran.stat.auckland.ac.nz/web/packages/MASS/) was used for logistic regression in the clinical features group. MCP-LASSO regression analysis was performed for radiomic features and combined predictors selection using the 'ncvreg' package (version 3.11.2; http://pbreheny.github.io/ncvreg) in R. The ROC curves were built using the 'pROC' (version 1.16.1; http://expasy.org/tools/pROC/) and 'ggplot2' (version 3.2.1; http://ggplot2.tidyverse.org) packages in R. The 'OptimalCutpoints' package (version 1.1-5; http://cran.stat.auckland.ac.nz/web/packages/OptimalCutpoints/) was used for cut-off calculation in R software. A nomogram was formulated using the package 'rms' (version 6.1-1; https://hbiostat.org/R/rms/) in R software. The concordance index (C-index), which represents the performance of the nomogram, was calculated with the 'rcorrcens' function present in the 'Hmisc' package (version 4.3-1; https://github.com/harrelfe/Hmisc) in R software. The ROC curves of the training cohort and validation cohort were compared by DeLong's test. $P<0.05$ was considered to indicate a statistically significant difference. The related computerized programs with R are listed in Appendix S1.

Results

Clinical features. A total of 184 patients were included in the present study (Fig. 1). Among these 184 patients, 10 presented two GGOs, while the remaining patients presented a single GGO, for a total of 194 GGOs. Of these 194 GGOs, 72 (including 21 AAH and 51 AIS) were in the preinvasive GGO group and 122 (including 31 MIA and 91 IA) were in the invasive GGO group. The clinical features of the two groups of patients were analysed (Table I) and there were no significant differences with regard to sex ($P=0.757$), age ($P=0.364$), smoking history ($P=0.725$), family history ($P=0.266$) or nodule location ($P=0.585$) between the preinvasive GGO and invasive GGO groups. However, there were significant differences in the maximum diameter ($P<0.001$) and consolidation ($P<0.001$) between the two groups. All the GGOs were divided

Table I. Clinical features of all patients.

Characteristics	Preinvasive GGO	Invasive GGO	Total	P-value[a]
Number of patients	72	122	194	
Sex, n (%)				0.757
Male	24 (35.3)	44 (64.7)	68	
Female	48 (38.1)	78 (61.9)	126	
Age, years[b]	59.1±1.05	60.31±8.19		0.364
Smoking history, n (%)				0.725
Non-smokers	54 (36.2)	95 (63.8)	149	
Smokers	18 (40.0)	27 (60.0)	45	
Family history, n (%)				0.266
No	61 (39.4)	94 (60.6)	155	
Yes	11 (28.2)	28 (71.8)	39	
Maximum_diameter, cm[b]	0.97±0.42	1.43±0.63		<0.001
Consolidation[b]	0.13±0.03	0.65±0.50		<0.001
Location, n (%)				0.585
Right upper	27 (37.5)	45 (62.5)	72	
Right middle	6 (54.5)	5 (45.5)	11	
Right low	9 (29.0)	22 (71.0)	31	
Left upper	21 (40.4)	31 (59.6)	52	
Left low	9 (32.1)	19 (67.9)	28	

[a]P-value was based on comparison between preinvasive group and invasive group. [b]Mean ± standard deviation. GGO, ground-glass opacity.

into two groups: i) The clinical training group, which included 136 patients who were hospitalized between January 2014 and January 2018, with 144 GGOs; and ii) the clinical validation cohort, which included 48 patients who were hospitalized between February 2018 and February 2019, with 50 GGOs.

Radiomic feature selection. Through TA of each patient's chest CT images, 851 radiomic features were obtained, including 107 original features and eight groups of wavelet features (each group contained 93 wavelet feature factors) obtained by decomposition of the original features (with the exception of 14 shape features). With an ICC >0.75 as the threshold, 613 stable radiomic features were identified, including 528 wavelet features and 85 original features (Fig. 2).

Clinical prediction model. The logistic regression analysis results revealed that consolidation was an independent predictor of invasiveness in the training cohort of 144 GGOs (P<0.001; Fig. 3). The ROC curve based on these plots was used to represent the clinical prediction model (clinical training cohort) of clinical features for the invasiveness of GGO. The cut-off value of consolidation was 0.23 cm (sensitivity, 0.681; specificity, 0.792; positive predictive value, 0.849; negative predictive value, 0.592; Fig. 3). The formula for calculating the clinical prediction model score was as follows: Clinical-score=-0.312+2.588 x consolidation.

Radiomic prediction model. After MCP-LASSO regression analysis and 10-fold cross-validation of 613 radiomic features in the clinical training cohort of 144 GGOs, two radiomic features, waveletHLL_ngtdm_Coarseness (P<0.01) and waveletLHH_firstorder_Maximum (P=0.01), were identified as independent predictors of invasiveness. ROC curves were drawn based on these radiomic features. In the prediction model, the AUCs of the texture features waveletHLL_ngtdm_Coarseness and waveletLHH_firstorder_Maximum were 0.692 (95% CI, 0.60-0.783) and 0.658 (95% CI, 0.557-0.758), respectively. The ability of a single texture feature to predict GGO invasiveness was poor. The combined predictive ability of all the texture features, radiomic training, was 0.719 (95% CI, 0.628-0.81), indicating improved predictive ability (Fig. 4). The formula for calculating the radiomic prediction model score was as follows: Radiomic-score=2.422-23.616 x waveletHLL_ngtdm_Coarseness-0.007 x waveletLHH_firstorder_Maximum.

Combined prediction model. Consolidation, waveletHLL_ngtdm_Coarseness, waveletLLH_glrlm_LongRunEmphasis and waveletLHH_firstorder_Maximum were selected from all the clinical and radiomic features by MCP-LASSO regression analysis and 10-fold cross-validation to construct the combined prediction model. The ROC curves are shown in Fig. 5. The combined prediction model score was calculated as follows: Combined-score=4.508+3.11 x consolidation-waveletHLL_ngtdm_Coarseness-0.827 x waveletHLL_glrlm_LongRunEmphasis-0.015 x waveletLHH_firstorder_Maximum.

The sensitivity, specificity, positive predictive value, negative predictive value, accuracy, AUC and 95% CI of each prediction model in the training cohort and validation cohort

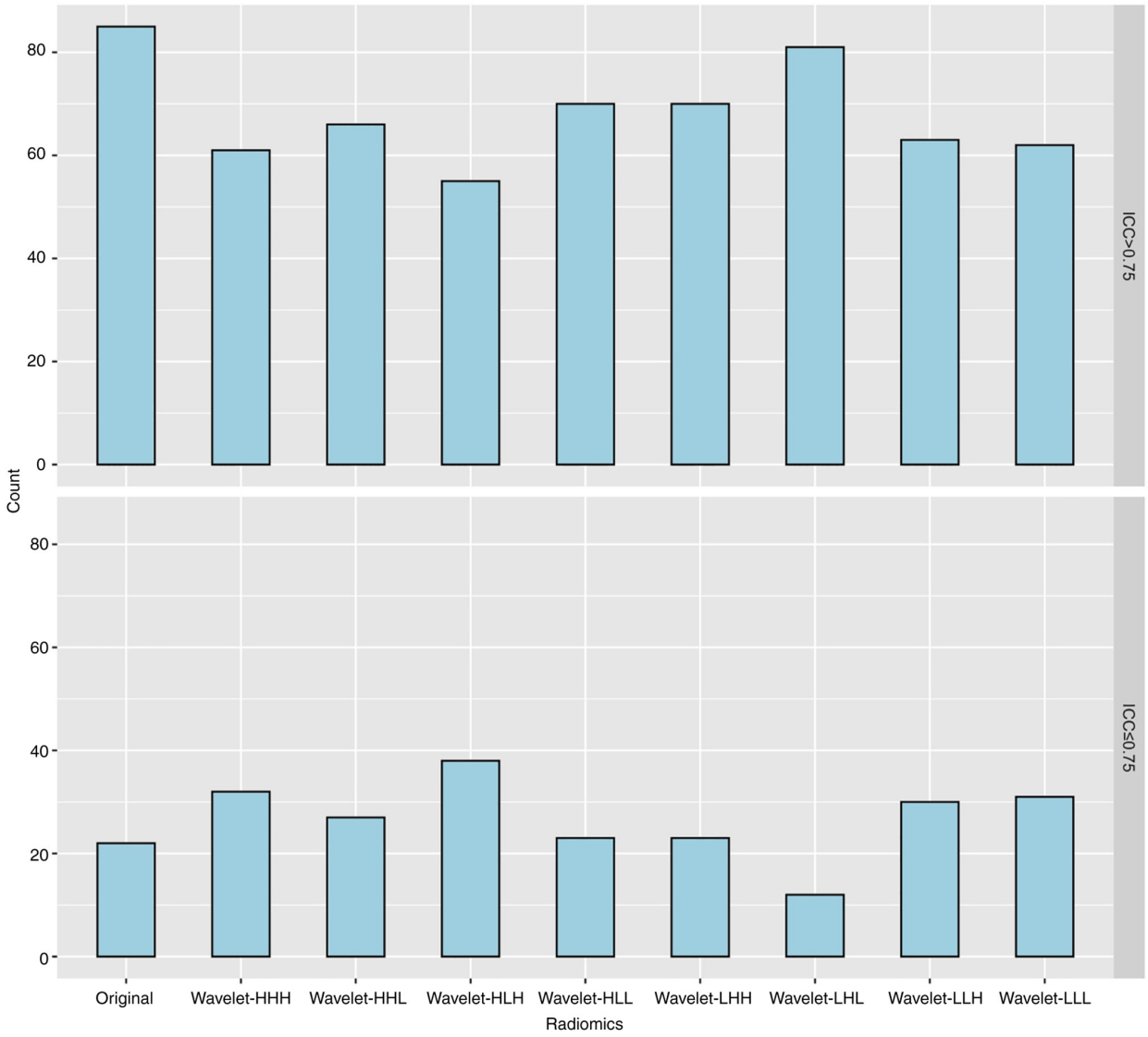

Figure 2. ICC histogram of all texture features. According to the size of the ICC, the texture features were divided into two groups: ICC >0.75 and ICC ≤0.75. ICC, intragroup correlation coefficient.

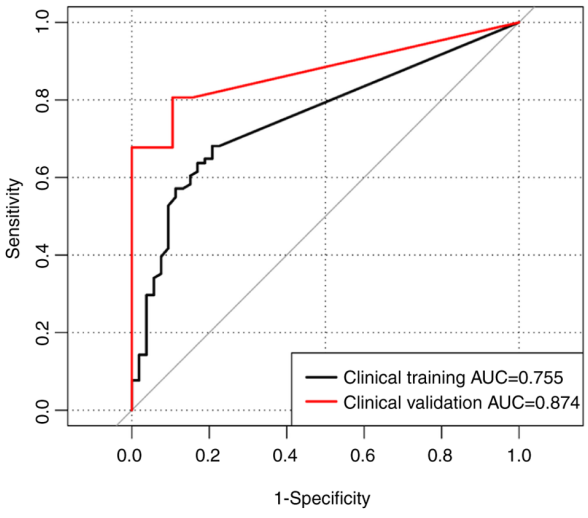

Figure 3. Clinical prediction model of ground-glass opacity invasion. The receiver operating characteristic curve for the training group (clinical training; AUC, 0.755) and validation group (clinical validation; AUC, 0.874). AUC, area under the curve.

were calculated to show the predictive ability (Table II). The predictive ability of the combined prediction model (AUC, 0.864; 95% CI, 0.802-0.926) was improved compared with that of any single prediction model developed with clinical (AUC, 0.755; 95% CI, 0.682-0.827) or radiomic (AUC, 0.719; 95% CI, 0.628-0.81) features.

Nomogram establishment and validation. Based on the four predictors selected in the combined model, a nomogram was constructed to predict the individual invasiveness of GGOs (Fig. 6). In the training cohort, the C-index of the invasion prediction nomogram was 0.864 (95% CI, 0.833-0.895), while it was 0.815 (95% CI, 0.905-0.969) in the verification cohort. The nomogram was subjected to 1,000 bootstrap resamples for internal validation and the calibration curve was plotted (Fig. 7). The mean absolute errors of the calibration curves were 0.027 in the training cohort and 0.031 in the validation cohort.

DCA. DCA is a method used to evaluate prediction models (26). The clinical decision curve was analysed based

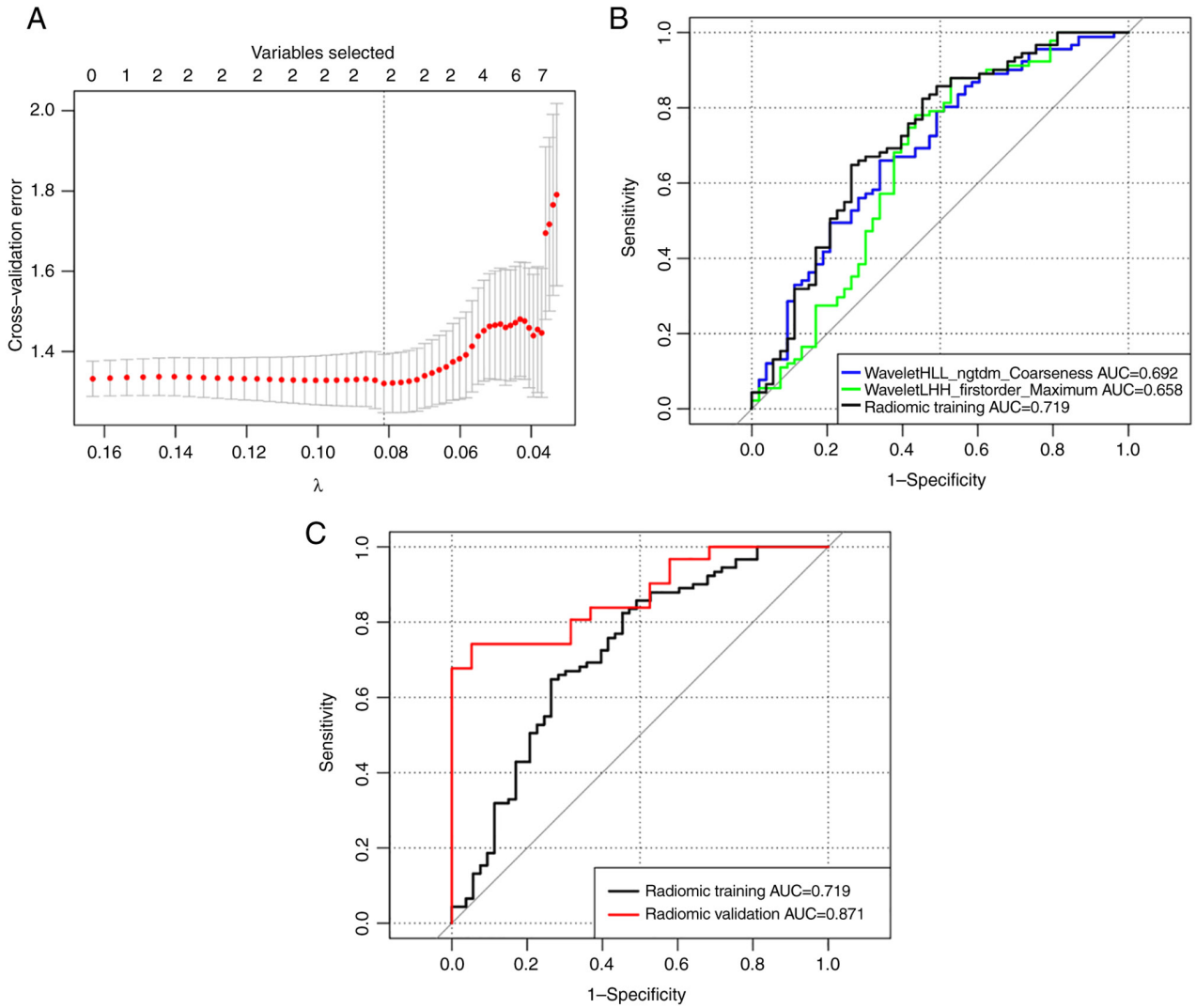

Figure 4. Radiomic feature selection and development of the radiomic prediction model. (A) The least absolute shrinkage and selection operator algorithm and 10-fold cross-validation for radiomic predictor selection. The optimal l value is 0.081 at the minimum cross-validation error (1.32) and the corresponding number of predictors is two. (B) ROC curve for invasiveness prediction with radiomic predictors alone and combined in the training cohort. (C) ROC curve for the training cohort (radiomic training) and validation cohort (radiomic validation) with corresponding AUCs of 0.719 and 0.871, respectively (P=0.025). AUC, area under the curve; ROC, receiver operating characteristic.

on the selected predictors (Fig. 8). A total of three predictive models of GGO invasiveness, namely the clinical, radiomic and combined models, were used in the training and verification groups. The results are presented in Fig. 8A and B, where the x-axis shows the threshold probability (Pt) and the y-axis shows the net benefit, which was calculated by adding the advantages (true-positive) and subtracting the disadvantages (false-positive). Within a large range of Pt values (20-90%; Fig. 8), the combined model has a greater net benefit than the clinical and radiomic models. For example, when the threshold probability was 45%, the net benefit rate was 46.7% in the combined model, 36.2% in the clinical model and 38.1% in the radiomic model. Therefore, the combined model has more clinical significance in predicting the invasiveness of GGOs.

Discussion

To date, it is still a challenge for thoracic surgeons to select the best treatment for pulmonary GGOs. The main reason is that it is difficult to classify GGOs before surgery, although a new classification of pulmonary adenocarcinoma was defined in 2011 (27). Preoperative percutaneous CT-guided fine-needle aspiration biopsy, endobronchial ultrasonography images and virtual bronchoscopy have been used for the pathological diagnosis of GGOs, but the diagnostic yield remains lower for smaller pGGOs (28,29). An increasing number of studies have focused on identifying imaging biomarkers for GGO classification through chest CT, especially for the identification of invasive GGO lesions (30-40).

On chest CT, preinvasive GGOs often appear as pGGOs, while invasive GGOs more often appear as larger, mixed GGOs (29-32). Eguchi *et al* (33) reported that if the diameter of a pGGO is >11 mm, it is likely to be invasive. Li *et al* (34) reported a cut-off diameter of 13.5 mm for evaluating the invasiveness of GGO nodules. In 2013, Lee *et al* (16) reported that the cut-off diameter for invasive GGOs was 14 mm. Another study published in 2019 reported that in the partly solid group of GGOs, a diameter >1 cm was a significant

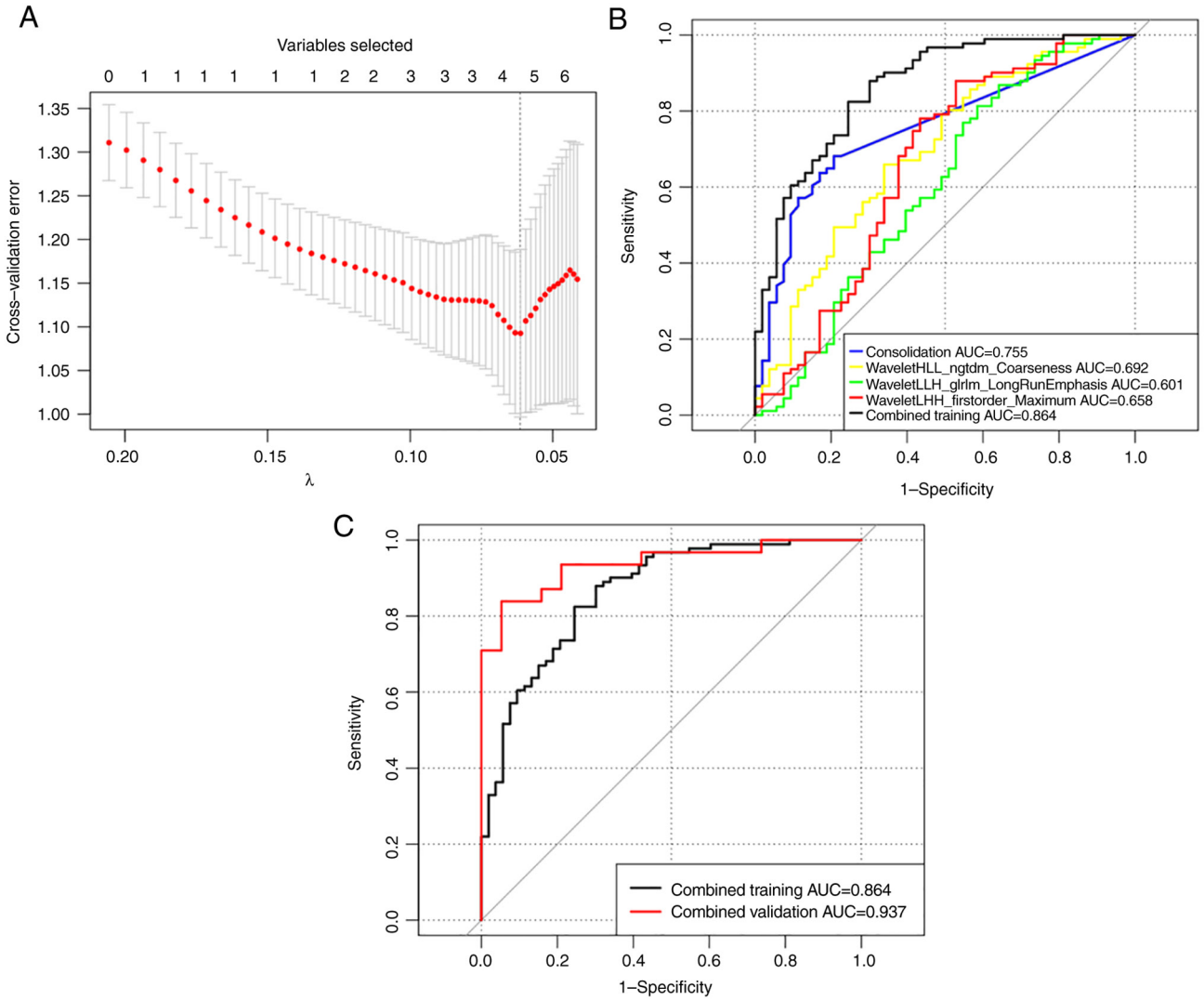

Figure 5. Development of the combined prediction model. (A) The least absolute shrinkage and selection operator algorithm and 10-fold cross-validation for combined predictor selection. When the minimum cross validation error is 1.09, the optimal l value is 0.061 and the corresponding number of non-zero coefficients is four. (B) ROC curves of the combined prediction model for the training cohort (combined training; AUC, 0.864) and the validation cohort (combined validation; AUC, 0.937). (C) ROC curves are shown to describe the discrimination of the clinical prediction model (clinical training), the general imaging prediction model (imaging training), the radiomic prediction model (radiomic training) and the combined prediction model (combined training). AUC, area under the curve; ROC, receiver operating characteristic.

factor for predicting invasiveness (35). A study performed on 232 patients and published in 2015 found that the solid component sizes with lung window setting (SCLW) and whole tumour sizes with mediastinal window setting (WTMV) were significantly correlated with tumour pathological invasion (36). The ROC curve analysis showed that for all subjects, the predictability of invasive results based on solid component size (such as SCLW and WTMV) was improved compared with that based on the whole tumour size (the maximum diameter of lung window tumour). This conclusion is in agreement with the results of the present study. However, the maximum tumour diameter was not an independent predictor of GGO invasion, while consolidation was an independent predictor of GGO invasion.

TA is an important type of medical image processing that can measure the tissue heterogeneity characteristics otherwise not observable by naked eyes, and can quantitatively display subtle changes in the image pixel values and arrangement (17). To the best of our knowledge, only a few studies have introduced TA and radiomic features of chest CT to the differentiation of invasive pulmonary GGOs. Chae *et al* (37) demonstrated that in part-solid GGOs, higher kurtosis and a smaller mass could significantly differentiate preinvasive lesions from invasive pulmonary adenocarcinomas (IPAs). Li *et al* (38) found that the voxel count and the correlation feature [correlation is a value between 0 (uncorrelated) and 1 (perfectly correlated) showing the linear dependency of gray level values to their respective voxels in the GLCM] were significant differentiators of preinvasive lesions from IPAs and MIAs. Another study in 2018 found that pGGOs or mixed lesions and fractal dimension were predictors of IAs that appear as GGOs (39). In another study, a support vector machine trained on all the heterogeneity indicators showed high accuracy (88.1%) in differentiating between indolent and invasive lesions (40). In these studies, only 2D or 3D original texture features were used and wavelet transform features

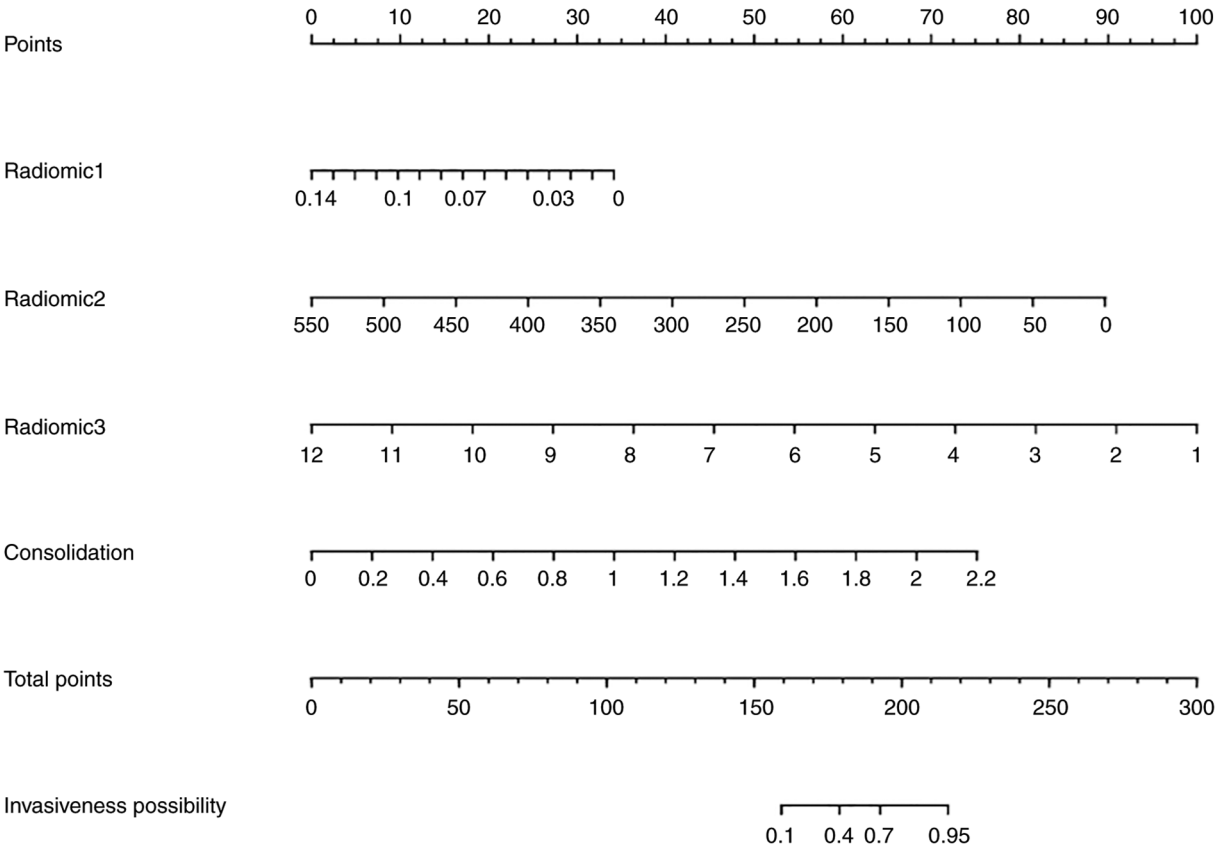

Figure 6. Nomogram that incorporated all the significant predictors of invasiveness is constructed with the training cohort. The predictors included radiomic1 (waveletHLL_ngtdm_Coarseness), radiomic2 (waveletLHH_firstorder_Maximum), Radiomic3 (waveletLLH_glrlm_LongRunEmphasis) and consolidation. The sum of points received for each variable value was located on the total points axis and a line was drawn downwards to the prediction axis to determine the probability of invasiveness.

were excluded. To the best of our knowledge, the present study is the first that enrolled 107 original features and eight groups of wavelet features (each group containing 93 wavelet feature factors) for radiomic predictor selection to differentiate the invasiveness of GGOs. For high-dimensional data, to avoid overfitting in the prediction, MCP-LASSO regression and 10-fold cross-validation analysis were used to identify relevant variables for the subsequent establishment of the radiomic prediction model. Finally, waveletHLL_ngtdm_Coarseness and waveletLHH_firstorder_Maximum were selected as independent predictors of invasiveness. Ngtdm_Coarseness is a measure of the average difference between the centre voxel and its neighbourhood, and is an indicator of the spatial change rate (41,42). A higher value indicates a lower spatial rate of change and a more uniform local texture. In the present study, the regression coefficient of waveletHLL_ngtdm_coarseness was -23.616, which indicated that the more uniform GGO the lower the probability of invasiveness. Firstorder_Maximum is the maximum grey intensity in the region of interest (43). The regression coefficient of waveletLHH_firstorder_Maximum was -0.007, which indicated that the smaller the maximum grey intensity of GGO the higher the probability of invasiveness. The AUCs of waveletHLL_ngtdm_Coarseness and waveletLHH_firstorder_Maximum were 0.692 (95% CI, 0.60-0.783) and 0.658 (95% CI, 0.557-0.758), respectively. However, the combination of the two radiomic predictors showed improved predictive ability for GGO invasion (training group: AUC, 0.719; 95% CI, 0.628-0.81; validation group: AUC, 0.87; 95% CI, 0.776-0.966).

In the combined prediction model for differentiating the invasiveness of GGOs, predictors were selected from all six clinical features and 613 stable radiomic features. Consolidation, waveletHLL_ngtdm_Coarseness, waveletLHH_firstorder_Maximum and waveletLLH_glrlm_LongRunEmphasis were considered. Glrlm_LongRunEmphais is a measure of the distribution of long run lengths, and it can reflect the distribution or adjacent relationships of pixels in the images (44). The regression coefficient of waveletLLH_glrlm_Longrunemphasis was -0.827, which indicated that GGOs with shorter long-range lengths and finer textures are more likely to be invasive. The predictive ability of the combined prediction model was improved compared with that of any single prediction model developed with clinical or radiomic features. The nomogram for the individual prediction model was constructed with the four predictors. Each GGO has a corresponding value of consolidation, waveletHLL_ngtdm_Coarseness, waveletLLH_glrlm_LongRunEmphasis and waveletLHH_firstorder_Maximum and the total score was calculated. In clinical application, the probability of the invasiveness of GGO with a total score >220 is >95% (Fig S1). Clinically, for such nodules, radical surgery such as lobectomy or segmental resection and lymph node dissection are preferred. For nodules with a total score <160, the probability of invasiveness is <10% (Fig S1). Clinically, regular

Table II. Diagnostic accuracy and AUC of prediction models.

Groups	Cohort	SEN, %	SPE, %	PPV, %	NPV, %	Accuracy, %	AUC	95% CI	P-value
Clinical	Training	68.1	79.2	84.9	59.2	72.2	0.755	0.682-0.827	0.04
	Validation	80.6	89.5	92.6	68.8	73.9	0.84	0.787-0.961	
Radiomic	Training	64.8	73.6	80.8	54.9	68.1	0.719	0.628-0.81	0.025
	Validation	74.2	94.7	95.8	69.2	82.0	0.871	0.776-0.966	
Combined	Training	82.4	75.5	85.2	71.4	79.9	0.864	0.802-0.926	0.109
	Validation	83.9	94.7	96.3	78.3	88.0	0.937	0.873-1.0	

SEN, sensitivity; SPE, specificity; PPV, positive predictive value; NPV, negative predictive value; AUC, area under curve.

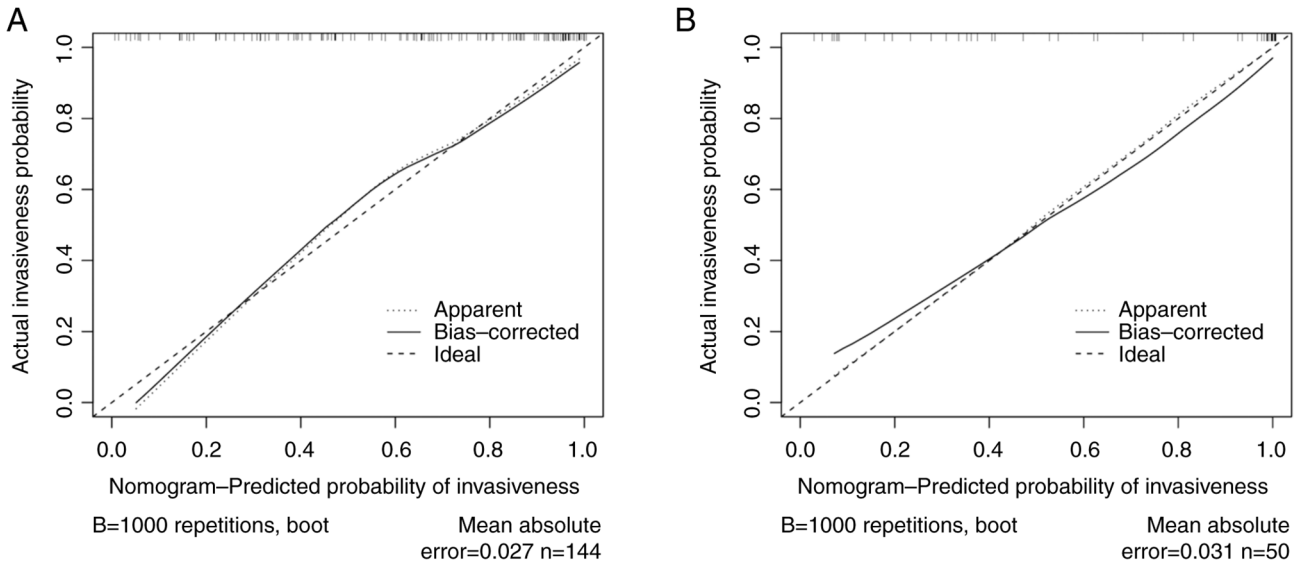

Figure 7. Calibration curve of the nomogram for predicting the probability of invasiveness. Probability of invasiveness in (A) the training cohort and (B) the validation cohort. The actual probability of invasiveness is plotted on the y-axis; the nomogram-predicted probability of invasiveness is plotted on the x-axis.

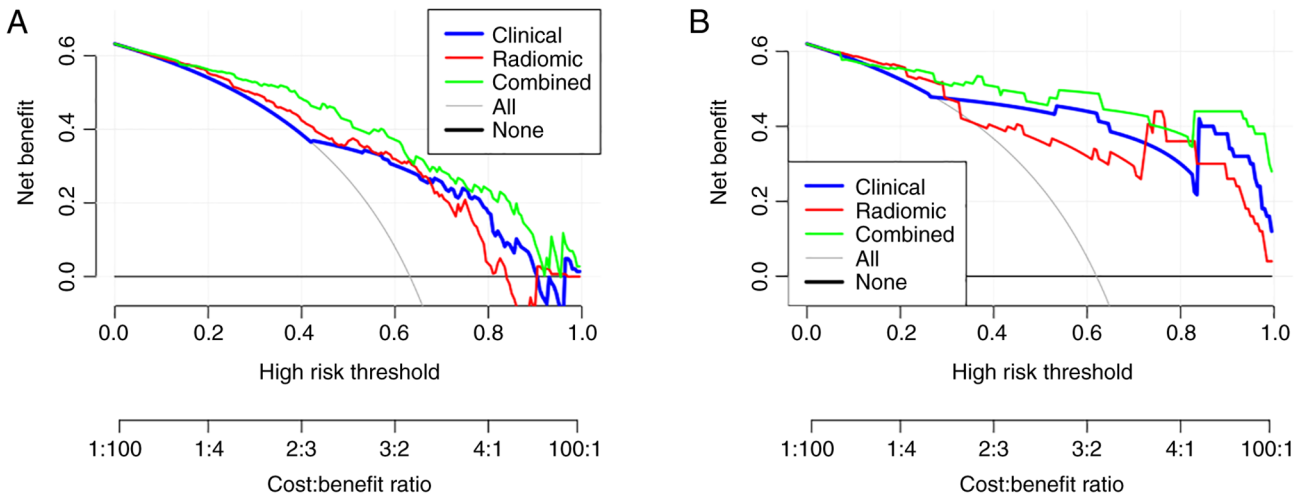

Figure 8. Clinical decision curve analysis. (A) Training and (B) validation group.

observation or localized resection are the main methods. The cutoff point of the nomogram is 0.5 and the corresponding total score is 185. The GGO can be diagnosed as having invasive potential GGO when the total score is >185. The C-index (training cohort: 0.864; 95% CI, 0.833-0.895; and validation cohort: 0.937; 95% CI, 0.905-0.969) and the calibration curve

showed that the nomogram used in the present study had good prediction ability.

Traditional diagnostic test indicators, such as sensitivity, specificity and AUC, only measure the diagnostic accuracy of the prediction model, but fail to consider the clinical utility of a specific model. The advantage of DCA is that it integrates the preferences of patients or decision makers into the analysis (26). In the present study, three predictive models of GGO invasiveness were analysed using DCA, and the combined model showed more clinical significance in predicting the invasiveness of GGOs.

The present study has some limitations. Due to the small sample size, the pGGO group was not analysed individually. Although we hypothesized that the maximum diameter and some radiomic features might show a good prediction ability for invasiveness in the pGGO group, this hypothesis needs to be confirmed by studies with larger sample sizes in the future.

In conclusion, the combined prediction model constructed with clinical and radiomic predictors showed a good ability to predict invasiveness in GGOs. The present study may help thoracic surgeons select the optimal treatment for patients with pulmonary GGOs.

Acknowledgements

Not applicable.

Funding

This study was supported by the Beijing Municipal Administration of Hospital Clinical Medicine Development of Special Funding Support (grant no. XMLX201702).

Availability of data and materials

The datasets used and/or analysed during the current study are available from the corresponding author on reasonable request. All codes used with R are available in Appendix S1.

Authors' contributions

YD was responsible for conceiving and designing the study, data analysis, writing of the manuscript and all manuscript revisions. RW and KQ were responsible for patient data collection and analysis. JL was responsible for CT data collection and editing of the manuscript. YZ was responsible for project conceptualization, manuscript revisions and editing of the manuscript. YD and YZ confirm the authenticity of all the raw data. All authors read and approved the final manuscript.

Ethics approval and consent to participate

The present study was approved by the Medical Research Ethics Committee of Shijingshan Hospital of Beijing City (Beijing, China; approval no. 2020-12). All the procedures involving human participants were performed in accordance with the ethical standards of both institutional and national research committees. Written informed consent was obtained before surgery from either the patients or their representatives.

Patient consent for publication

Not applicable.

Competing interests

The authors declare that they have no competing interests.

References

1. Tsutsui S, Ashizawa K, Minami K, Tagawa T, Nagayasu T, Hayashi T and Uetani M: Multiple focal pure ground-glass opacities on high-resolution CT images: Clinical significance in patients with lung cancer. AJR Am J Roentgenol 195: W131-W138, 2010.
2. Miller A, Markowitz S, Manowitz A and Miller JA: Lung cancer screening using low-dose high-resolution CT scanning in a high-risk workforce: 3500 nuclear fuel workers in three US states. Chest 125 (Suppl 5): 152S-153S, 2004.
3. Migliore M, Fornito M, Palazzolo M, Criscione A, Gangemi M, Borrata F, Vigneri P, Nardini M and Dunning J: Ground glass opacities management in the lung cancer screening era. Ann Transl Med 6: 90, 2018.
4. Ye T, Deng L, Xiang J, Zhang Y, Hu H, Sun Y, Li Y, Shen L, Wang S, Xie L and Chen H: Predictors of pathologic tumor invasion and prognosis for ground glass opacity featured lung adenocarcinoma. Ann Thorac Surg 106: 1682-1690, 2018.
5. Travis WD, Brambilla E, Noguchi M, Nicholson AG, Geisinger KR, Yatabe Y, Beer DG, Powell CA, Riely GJ, Van Schil PE, *et al*: International association for the study of lung cancer/American thoracic society/European respiratory society international multidisciplinary classification of lung adenocarcinoma. J Thorac Oncol 6: 244-285, 2011.
6. Dai J, Yu G and Yu J: Can CT imaging features of ground-glass opacity predict invasiveness? A meta-analysis. Thorac Cancer 9: 452-458, 2018.
7. Park CM, Goo JM, Lee HJ, Lee CH, Kim HC, Chung DH and Im JG: CT findings of atypical adenomatous hyperplasia in the lung. Korean J Radiol 7: 80-86, 2006.
8. Nagao M, Murase K, Yasuhara Y, Ikezoe J, Eguchi K, Mogami H, Mandai K, Nakata M and Ooshiro Y: Measurement of localized ground-glass attenuation on thin-section computed tomography images: Correlation with the progression of bronchioloalveolar carcinoma of the lung. Invest Radiol 37: 692-697, 2002.
9. Van Schil PE, Asamura H, Rusch VW, Mitsudomi T, Tsuboi M, Brambilla E and Travis WD: Surgical implications of the new IASLC/ATS/ERS adenocarcinoma classification. Eur Respir J 39: 478-486, 2012.
10. Koike T, Togashi K, Shirato T, Sato S, Hirahara H, Sugawara M, Oguma F, Usuda H and Emura I: Limited resection for noninvasive bronchioloalveolar carcinoma diagnosed by intraoperative pathologic examination. Ann Thorac Surg 88: 1106-1111, 2009.
11. Pedersen JH, Saghir Z, Wille MM, Thomsen LH, Skov BG and Ashraf H: Ground-glass opacity lung nodules in the era of lung cancer CT screening: Radiology, pathology and clinical management. Oncology (Williston Park) 30: 266-274, 2016.
12. Chou HP, Lin KH, Huang HK, Lin LF, Chen YY, Wu TH, Lee SC, Chang H and Huang TW: Prognostic value of positron emission tomography in resected stage IA non-small cell lung cancer. Eur Radiol 31: 8021-8029, 2021.
13. Inoue M, Minami M, Sawabata N, Utsumi T, Kadota Y, Shigemura N and Okumura M: Clinical outcome of resected solid-type small-sized c-stage IA non-small cell lung cancer. Eur J Cardiothorac Surg 37: 1445-1449, 2010.
14. Higuchi M, Yaginuma H, Yonechi A, Kanno R, Ohishi A, Suzuki H and Gotoh M: Long-term outcomes after video-assisted thoracic surgery (VATS) lobectomy versus lobectomy via open thoracotomy for clinical stage IA non-small cell lung cancer. J Cardiothorac Surg 9: 88, 2014.
15. Zhang J, Wu J, Tan Q, Zhu L and Gao W: Why do pathological stage IA lung adenocarcinomas vary from prognosis?: A clinicopathologic study of 176 patients with pathological stage IA lung adenocarcinoma based on the IASLC/ATS/ERS classification. J Thorac Oncol 8: 1196-1202, 2013.

16. Lee SM, Park CM, Goo JM, Lee HJ, Wi JY and Kang CH: Invasive pulmonary adenocarcinomas versus preinvasive lesions appearing as ground-glass nodules: Differentiation by using CT features. Radiology 268: 265-273, 2013.
17. Lambin P, Rios-Velazquez E, Leijenaar R, Carvalho S, van Stiphout RGPM, Granton P, Zegers CML, Gillies R, Boellard R, Dekker A and Aerts HJWL: Radiomics: Extracting more information from medical images using advanced feature analysis. Eur J Cancer 48: 441-446, 2012.
18. Wilson R and Devaraj A: Radiomics of pulmonary nodules and lung cancer. Transl Lung Cancer Res 6: 86-91, 2017.
19. Han F, Wang H, Zhang G, Han H, Song B, Li L, Moore W, Lu H, Zhao H and Liang Z: Texture feature analysis for computer-aided diagnosis on pulmonary nodules. J Digit Imaging 28: 99-115, 2015.
20. Kumar V, Gu Y, Basu S, Berglund A, Eschrich SA, Schabath MB, Forster K, Aerts HJWL, Dekker A, Fenstermacher D, *et al*: Radiomics: The process and the challenges. Magn Reson Imaging 30: 1234-1248, 2012.
21. Zhao S, Ren W, Zhuang Y and Wang Z: The influence of different segmentation methods on the extraction of imaging histological features of hepatocellular carcinoma CT. J Med Syst 43: 1-7, 2019.
22. Çinarer G, Gürsel B and Haşim A: Prediction of glioma grades using deep learning with wavelet radiomic features. Appl Sci 10: 6296, 2020.
23. Korpershoek YJ, Slot JC, Effing TW, Schuurmans MJ and Trappenburg JC: Self-management behaviors to reduce exacerbation impact in COPD patients: A Delphi study. Int J Chron Obstruct Pulmon Dis 12: 2735-2746, 2017.
24. Dang Y, Wang R, Qian K, Lu J, Zhang H and Zhang Y: Clinical and radiological predictors of epidermal growth factor receptor mutation in nonsmall cell lung cancer. J Appl Clin Med Phys 22: 271-280, 2021.
25. Dong M, Hou G, Li S, Li N, Zhang L and Xu K: Preoperatively estimating the malignant potential of mediastinal lymph nodes: A pilot study toward establishing a robust radiomics model based on contrast-enhanced CT imaging. Front Oncol 10: 558428, 2021.
26. Vickers AJ and Elkin BB: Decision curve analysis: A novel method for evaluating prediction models. Med Decis Making 26: 565-574, 2006.
27. Sun F, Xi J, Zhan C, Yang X, Wang L, Shi Y, Jiang W and Wang Q: Ground glass opacities: Imaging, pathology, and gene mutations. J Thorac Cardiovasc Surg 156: 808-813, 2018.
28. Shimizu K, Ikeda N, Tsuboi M, Hirano T and Kato H: Percutaneous CT- guided fine needle aspiration for lung cancer smaller than 2 cm and revealed by ground-glass opacity at CT. Lung Cancer 51: 173-179, 2006.
29. Ikezawa Y, Shinagawa N, Sukoh N, Morimoto M, Kikuchi H, Watanabe M, Nakano K, Oizumi S and Nishimura M: Usefulness of endobronchial ultrasonography with a guide sheath and virtual bronchoscopic navigation for ground-glass opacity lesions. Ann Thorac Surg 103: 470-475, 2017.
30. Zhang Y, Qiang JW, Ye JD, Ye XD and Zhang J: High resolution CT in differentiating minimally invasive component in early lung adenocarcinoma. Lung Cancer 84: 236-241, 2014.
31. Lee HJ, Lee CH, Jeong YJ, Chung DH, Goo JM, Park CM and Austin JHM: IASLC/ATS/ERS international multidisciplinary classification of lung adenocarcinoma: Novel concepts and radiologic implications. J Thorac Imaging 27: 340-353, 2012.
32. Kobayashi Y, Ambrogio C and Mitsudomi T: Ground-glass nodules of the lung in never-smokers and smokers: Clinical and genetic insights. Transl Lung Cancer Res 7: 487-497, 2018.
33. Eguchi T, Yoshizawa A, Kawakami S, Kumeda H, Umesaki T, Agatsuma H, Sakaizawa T, Tominaga Y, Toishi M and Hashizume M: Tumor size and computed tomography attenuation of pulmonary pure ground-glass nodules are useful for predicting pathological invasiveness. PLoS One 9: e97867, 2014.
34. Li M, Wang Y, Chen Y and Zhang Z: Identification of preoperative prediction factors of tumor subtypes for patients with solitary ground-glass opacity pulmonary nodules. J Cardiothorac Surg 13: 9, 2018.
35. Chen PH, Chang KM, Tseng WC, Chen CH and Chao JI: Invasiveness and surgical timing evaluation by clinical features of ground-glass opacity nodules in lung cancers. Thorac Cancer 10: 2133-2141, 2019.
36. Saji H, Matsubayashi J, Akata S, Shimada Y, Kato Y, Kudo Y, Nagao T, Park J, Kakihana M, Kajiwara N, *et al*: Correlation between whole tumor size and solid component size on high-resolution computed tomography in the prediction of the degree of pathologic malignancy and the prognostic outcome in primary lung adenocarcinoma. Acta Radiol 56: 1187-1195, 2015.
37. Chae HD, Park CM, Park SJ, Lee SM, Kim KG and Goo JM: Computerized texture analysis of persistent part-solid ground-glass nodules: Differentiation of preinvasive lesions from invasive pulmonary adenocarcinomas. Radiology 273: 285-293, 2014.
38. Li W, Wang X, Zhang Y, Li X, Li Q and Ye Z: Radiomic analysis of pulmonary ground-glass opacity nodules for distinction of preinvasive lesions, invasive pulmonary adenocarcinoma and minimally invasive adenocarcinoma based on quantitative texture analysis of CT. Chin J Cancer Res 30: 415-424, 2018.
39. Xue X, Yang Y, Huang Q, Cui F, Lian Y, Zhang S, Yao L, Peng W, Li X, Pang P, *et al*: Use of a radiomics model to predict tumor invasiveness of pulmonary adenocarcinomas appearing as pulmonary ground-glass nodules. Biomed Res Int 2018: 6803971, 2018.
40. Li M, Narayan V, Gill RR, Jagannathan JP, Barile MF, Gao F, Bueno R and Jayender J: Computer-aided diagnosis of ground-glass opacity nodules using open-source software for quantifying tumor heterogeneity. Am J Roentgenol 209: 1216-1227, 2017.
41. Haralick RM, Shanmugam K and Dinstein I: Textural features for image classification. IEEE Trans Systems Man Cybernetics 6: 610-621, 1973.
42. Zhang Y, Ko CC, Chen JH, Chang KT, Chen TY, Lim SW, Tsui YK and Su MY: Radiomics approach for prediction of recurrence in non-functioning pituitary macroadenomas. Front Oncol 10: 590083, 2020.
43. Batur A, Kılınçer A, Ateş F, Demir NA and Ergün R: Evaluation of systemic involvement of Coronavirus disease 2019 through spleen; size and texture analysis. Turk J Med Sci 51: 972-980, 2021.
44. Chen ZW, Tang K, Zhao YF, Chen YZ, Tang LJ, Li G, Huang OY, Wang XD, Targher G, Byrne CD, *et al*: Radiomics based on fluoro-deoxyglucose positron emission tomography predicts liver fibrosis in biopsy-proven MAFLD: A pilot study. Int J Med Sci 18: 3624-3630, 2021.